J|A|C|S ARTICLES

Published on Web 06/10/2010

A Molecular $Ce_2@I_h$-C_{80} Switch—Unprecedented Oxidative Pathway in Photoinduced Charge Transfer Reactivity

Dirk M. Guldi,*,† Lai Feng,‡,§ Shankara Gayathri Radhakrishnan,† Hidefumi Nikawa,‡ Michio Yamada,‡ Naomi Mizorogi,‡ Takahiro Tsuchiya,‡ Takeshi Akasaka,‡ Shigeru Nagase,⊥ M. Ángeles Herranz,|| and Nazario Martín||

Department of Chemistry and Pharmacy & Interdisciplinary Center for Molecular Materials, Friedrich-Alexander-Universität Erlangen-Nürnberg, 91058 Erlangen, Germany, Center for Tsukuba Advanced Research Alliance, University of Tsukuba, Tsukuba 305-8577, Japan, Institute of Chemistry, Chinese Academy of Sciences, Beijing 100080, China, Department of Theoretical and Computational Molecular Science, Institute for Molecular Science, Okazaki 444-8585, Japan, and Departamento de Química Orgánica, Facultad de Química, Universidad Complutense, E-28040 Madrid, Spain

Received March 13, 2010; E-mail: guldi@chemie.uni-erlangen.de

Abstract: We report for the first time the versatile $Ce_2@I_h$-C_{80} building block toward synthesizing a novel electron donor−acceptor conjugate, $Ce_2@I_h$-C_{80}-ZnP (**1**). A systematic investigation of the charge transfer chemistry documents a *reductive charge transfer* (i.e., formation of $(Ce_2@I_h\text{-}C_{80})^{\bullet-}$-$(ZnP)^{\bullet+}$) in nonpolar media (i.e., toluene/THF), while an *oxidative charge transfer* (i.e., formation of $(Ce_2@I_h\text{-}C_{80})^{\bullet+}$-$(ZnP)^{\bullet-}$) dominates in polar media (i.e., benzonitrile/DMF). Reduction of the $[Ce_2]^{6+}$ cluster, which is highly localized and collinearly arranged with respect to the quaternary bridge carbon, is sufficiently exothermic in all solvents. Notably weak is the electronic coupling between the $[Ce_2]^{6+}$ cluster and the electron-donating ZnP. The oxidation of C_{80}^{6-} and the simultaneous reduction of ZnP, on the other hand, necessitate solvent stabilization. In such a case, the strongly exothermic $(Ce_2@I_h\text{-}C_{80})^{\bullet-}$-$(ZnP)^{\bullet+}$ radical ion pair state formation is compensated within the framework of a nonadiabatic charge transfer by a C_{80}^{6-}/ZnP electronic matrix element, as the sum of good overlap and short distance, that exceeds that for $[Ce_2]^{6+}$/ZnP.

Introduction

In recent years, the great versatility of empty fullerenes, especially as integrative building blocks in electron donor−acceptor conjugates/hybrids, has been established.[1] Empty fullerenes exhibit all of the hallmarks that are found in nature's most sophisticated and important solar energy conversion/storage systems, namely, photosynthetic organisms in plants, algae, and a variety of types of bacteria.[2] Owing to its rigid structure, C_{60} possesses small reorganization energies in charge transfer reactions, which is of particular interest and which, as a matter of fact, has exerted noteworthy impact on the improvement of charge separation processes triggered by light.[3] The oxidation of C_{60} requires strong chemical, photochemical, or pulse radiolytical oxidants. Still, direct oxidative charge transfer within C_{60} electron donor−acceptor systems has not been observed.[4]

Endohedral metallofullerenes (i.e., $M_n@C_{2m}$; $n = 1-2$ and $m = 30-50$) bear, in contrast to empty fullerenes, additional atoms, ions, or clusters within their inner spheres. What renders endohedral metallofullerenes particularly appealing is that a significant control over the chemical and physical properties has been realized by just changing the nature and composition of the encapsulated species.[5] For instance, $M_2@I_h$-C_{80} (M = Ce or La)[6] reveal, in stark contrast to empty fullerenes, strong electron-accepting and electron-donating features.[7] To this end, $M_2@C_{80}$ is expected to emerge as an adjustable building block

† Friedrich-Alexander-Universität Erlangen-Nürnberg.
‡ University of Tsukuba.
§ Chinese Academy of Sciences.
⊥ Institute for Molecular Science.
|| Universidad Complutense.

(1) (a) Yu, G.; Gao, J.; Hummelen, J. C.; Wudl, F.; Heeger, A. J. *Science* **1995**, *270*, 1789–1791. (b) Rand, B. P.; Xue, J.; Uchida, S.; Forrest, S. R. *J. Appl. Phys.* **2005**, *98*, 124902. (c) Peet, J.; Heeger, A. J.; Bazan, G. C. *Acc. Chem. Res.* **2009**, *42*, 1700–1708.
(2) Collings, A. F.; Critchley, C. *Artificial Photosynthesis: From Basic Biology to Industrial Application*; Wiley-VCH: Weinheim, Germany, 2005.
(3) Gust, D.; Moore, T. A.; Moore, A. L. *Acc. Chem. Res.* **2009**, *42*, 1890–1898.
(4) Ohkubo, K.; Ortiz, J.; Martín-Gomis, L.; Fernández-Lázaro, F.; Sastre-Santos, Á.; Fukuzumi, S. *Chem. Commun.* **2007**, 589–591.
(5) *Endofullerenes: A New Family of Carbon Clusters*; Akasaka, T., Nagase, S., Eds.; Kluwer: Dordrecht, The Netherlands, 2002.
(6) (a) Suzuki, T.; Maruyama, Y.; Kato, T.; Kikuchi, K.; Nakao, Y.; Achiba, Y.; Kobayashi, K.; Nagase, S. *Angew. Chem.* **1995**, *107*, 1228; *Angew. Chem., Int. Ed. Engl.* **1995**, *34*, 1094−1096. (b) Ding, J.; Yang, S. *Angew. Chem.* **1996**, *108*, 2369; *Angew. Chem., Int. Ed. Engl.* **1996**, *35*, 2234−2235. (c) Akasaka, T.; Nagase, S.; Kobayashi, K.; Waelchli, M.; Yamamoto, K.; Funasaka, H.; Kako, M.; Hoshino, T.; Erata, T. *Angew. Chem.* **1997**, *109*, 1716; *Angew. Chem., Int. Ed. Engl.* **1997**, *36*, 1643−1645. (d) Nishibori, E.; Takata, M.; Sakata, M.; Taninaka, A.; Shinohara, H. *Angew. Chem.* **2001**, *113*, 3086; *Angew. Chem., Int. Ed.* **2001**, *40*, 2998−2999. (e) Shimotani, H.; Ito, T.; Iwasa, Y.; Taninaka, A.; Shinohara, H.; Nishibori, E.; Takata, M.; Sakata, M. *J. Am. Chem. Soc.* **2004**, *126*, 364–369.
(7) Tsuchiya, T.; Akasaka, T.; Nagase, S. *Bull. Chem. Soc. Jpn.* **2009**, *82*, 171–181.

10.1021/ja101856j

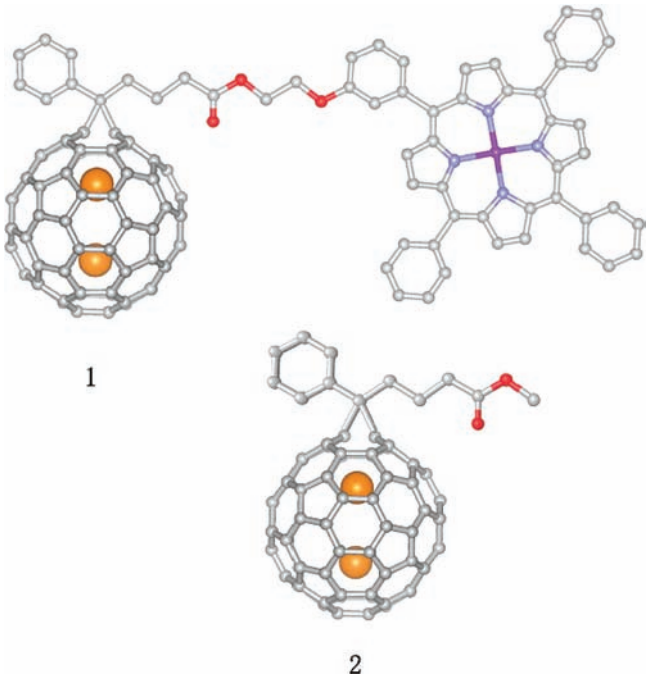

Figure 1. Structures of $Ce_2@I_h$-C_{80}-ZnP (**1**) and $Ce_2@I_h$-PCBM (**2**).

that takes on the role of either an electron acceptor (i.e., applicable toward the reduction of CO_2) or an electron donor (i.e., applicable toward the oxidation of water). Here, we report for the first time using $M_2@I_h$-C_{80} toward synthesizing a unique $M_2@I_h$-C_{80} containing an electron donor−acceptor conjugate, $Ce_2@I_h$-C_{80}-ZnP (**1**) (Figure 1). A systematic investigation of the charge transfer chemistry documents the malleable features of $Ce_2@I_h$-C_{80}, that is, giving rise to *reductive charge transfer* in nonpolar media, while *oxidative charge transfer* dominates in polar media. Key to the charge transfer outcome is a fine balance in the thermodynamic driving force and in electronic coupling. Thus, the use of endohedral metallofullerenes as an *electron donor* in electron donor−acceptor conjugates opens new avenues for carbon-based materials in the context of charge transfer processes and photovoltaic applications, especially considering that, so far, fullerenes act solely as electron acceptors in photo- and redox-active electron donor−acceptor conjugates.

Results and Discussion

Endohedral metallofullerenes possess reduction potentials comparable to that of C_{60}, C_{70}, C_{84}, etc. Additionally, unlike the latter, their oxidation potentials are close to those of widely used electron donors such as metalloporphyrins, tetrathiafulvalenes, etc.[5,7] As a consequence of encapsulating a dimetallic cluster (i.e., $[M_2]^{6+}$ cluster), $M_2@I_h$-C_{80} has 86 π-electrons−80 plus 6 π-electrons from C_{80}^{6-} and $[M_2]^{6+}$, respectively.[8] Such a feature is important for stabilizing unusual redox states under both reductive and oxidative conditions. In this light, we designed a strategy to link $Ce_2@I_h$-C_{80} to a zinc tetraphenylporphyrin (i.e., ZnP) via a flexible 2-oxyethyl butyrate spacer. ZnP with its broad absorption cross section in the visible range of the solar spectrum generates compelling excited states that are either strong oxidants or strong reductants. In short, $Ce_2@I_h$-C_{80}-ZnP (**1**) should satisfy all the criteria necessary to switch the charge transfer activity, that is, from a reductive to an oxidative mechanism, which are controlled by solvent polarity.

Figure 2. ORTEP view of one of the enantiomers of **2**; the solvent molecules (i.e., CS_2) are omitted for clarity.

The syntheses of references **2** and **1** were carried out via a [2 + 1]-cycloaddition reaction[9] of diazo precursors[10] with $Ce_2@I_h$-C_{80} affording **2** and **1** as major products. MALDI-TOF mass spectrometry confirmed the integrity of **2** and **1** with molecular ion peaks of *m*/*z* 1429.52 and 2136.18, respectively. Importantly, single-crystal X-ray analyses, as shown in Figure 2, shed light onto the structure of **2**, namely, a [6,6]-fulleroid.[11] Additional evidence for the [6,6]-fulleroid structure came from ^{13}C NMR studies, which illustrate that in **2** the original π-system of $Ce_2@I_h$-C_{80} is sustained. Notable, this feature contrasts the [6,6]-methanofullerene structure of C_{60}, where the number of π-electrons is reduced to 58.[9a] The $[Ce_2]^{6+}$ cluster is highly localized and collinearly arranged relative to the quaternary bridge carbon of C_{80}^{6-}, much like that in previously reported carbene adducts of $La_2@I_h$-C_{80}.[12]

The structures of **2** and **1** were further corroborated by NMR studies, including ^1H NMR, ^{13}C NMR, COSY, and HMQC experiments. Notable are the following magnetic features of **2** and **1**. First, **2** and **1** are paramagnetic owing to the two f-electrons of the $[Ce_2]^{6+}$ cluster.[8] Second, **2** and **1** are magnetically anisotropic due to magnetic dipole interactions operative between the $[Ce_2]^{6+}$ cluster, on one hand, and the

(8) (a) Kobayashi, K.; Nagase, S. *Chem. Phys. Lett.* **1996**, *262*, 227–232. (b) Yamada, M.; Mizorogi, N.; Tsuchiya, T.; Akasaka, T.; Nagase, S. *Chem.—Eur. J.* **2009**, *15*, 9486–9493.

(9) (a) Hummelen, J. C.; Knight, B. W.; LePeq, F.; Wudl, F.; Yao, J.; Wilkins, C. L. *J. Org. Chem.* **1995**, *60*, 532–538. (b) Ross, R. B.; Cardona, C. M.; Guldi, D. M.; Gayathri, S. S.; Reese, M. O.; Kopidakis, N.; Peet, J.; Walker, B.; Bazan, G. C.; Van Keuren, E.; Holloway, B. C.; Drees, M. *Nat. Mater.* **2009**, *8*, 208–212. (c) Shu, C.; Xu, W.; Slebodnick, C.; Champion, H.; Fu, W.; Reid, J. E.; Azurmendi, H.; Wang, C.; Harick, K.; Dorn, H. C.; Gibson, H. W. *Org. Lett.* **2009**, *11*, 1753–1756.

(10) See Supporting Information.

(11) Crystal data for **2**·$2CS_2$: $C_{94}H_{14}Ce_2O_2S_4$, M_r = 1583.53, black plate, 0.41 × 0.30 × 0.04 mm, monoclinic, space group $P2_1/c$, a = 14.5938(15) Å, b = 11.0075(9) Å, c = 32.940(3) Å, β = 99.129(4)°, V = 5224.5(9) Å^3, Z = 4; ρ_{calcd} = 2.018 g cm^{-3}, μ(Mo Kα) = 1.951 mm^{-1}, θ_{max} = 32.030, T = 120 K, 83 764 total collected reflections, 18 107 unique reflections, 1112 refined parameters, GOF = 1.118, R_1 = 0.0994 and wR_2 = 0.2653 for all data; R_1 = 0.0901 for 15 772 independent reflections ($I > 2.0\sigma(I)$), min/max electron density 7.840/−5.396 eÅ^{-3}.

(12) Yamada, M.; Someya, C.; Wakahara, T.; Tsuchiya, T.; Maeda, Y.; Akasaka, T.; Yoza, K.; Horn, E.; Liu, M. T. H.; Mizorogi, N.; Nagase, S. *J. Am. Soc. Chem.* **2008**, *130*, 1171–1176.

Table 1. Partial ^{1}H NMR Chemical Shifts (ppm) of **2** and **1** (300 MHz, in $C_2D_2Cl_4$, 293 K)

	$Ar_{para\text{-}H}$[a] (P4)	$Ar_{meta\text{-}H'}$ (P5)	$Ar_{meta\text{-}H}$ (P3)	$Ar_{ortho\text{-}H'}$ (P6)	$Ar_{ortho\text{-}H}$ (P2)	CH_2CO_2 (S3)	CCH_2CH_2 (S2a/b)	$ArCCH_2$ (S1a/b)
2	4.04	2.98	2.41	−5.12	−6.34	−3.28	−10.17/−9.79	−18.10/−17.60
1	4.10	3.13	2.57	−4.87	−6.09	−3.43	−10.09/−9.74	−17.96/−17.43

[a] Ar refers to the phenyl group that is next to the bridgehead carbon in **2** and **1**.

protons and carbons outside the C_{80}^{6-} cage, on the other hand.[13] Finally, the chemical shifts of all protons (**2** and **1**) depend, in part, on their geometrical positions relative to the $[Ce_2]^{6+}$ cluster, which is described by eq 1.[14]

$$\delta = \delta_{\text{dia}} + \sum_{i=\text{Ce(1)},\text{Ce(2)}} \frac{C(3\cos^2\theta_i - 1)}{\gamma_i^3}\frac{1}{T^2} \qquad (1)$$

Therefore, it is not unexpected that the presence of unpaired f-electrons (i.e., $[Ce_2]^{6+}$ cluster) evokes distinguished upfield shifts of the phenyl as well as the methylene protons (**2** and **1**). Overall, significant similarities in the chemical shifts (see Table 1) reflect the structural similarity between **2** and **1**. Notable is the separation of the *ortho*- and *meta*-phenyl protons at 293 K: $\Delta\delta_{o\text{-}ArH} = 1.22$ ppm and $\Delta\delta_{m\text{-}ArH} = 0.56$ ppm (Figure S4 in the Supporting Information and Figure 3a). The latter implies rotations of the phenyl groups that are much slower than the ^{1}H NMR time scale. The geminal methylene protons (S1a/b and S2a/b) adjacent to the quaternary bridge carbon are also affected. Their chemical shifts differ by ca. 0.5 and 0.4 ppm, respectively, suggesting different magnetic environments. The overall difference vanishes, however, as the distance between the methylene/methyl protons and C_{80}^{6-} increases. Implicit is that both the anisotropism of magnetic field imparted by the $[Ce_2]^{6+}$ cluster and the shielding from either the five- or six-membered rings[15] fall off sharply with distance.

Variable-temperature NMR experiments from 283 to 308 K were performed to dissect possible $Ce_2@I_h$-C_{80}/ZnP intramolecular interactions. Figure 3b and Figure S7c (Supporting Information) document that within the 6−12 ppm window a total of 26 ^{1}H signals emerged. With the help of 2D-DQFCOSY, NOESY, and HSQC experiments (i.e., 293 and/or 283 K), all these ^{1}H signals were unambiguously assigned to the porphyrin protons (27*H*).[10] The diagnostic NOE correlations between the methylene protons (S6) and the phenyl protons (5b/5d) of ZnP were taken as spectroscopic evidence for the linking of the spacer to ZnP.[10] It should be noted that the chemical shifts of (i) the β-pyrrole protons, (ii) the *ortho*-, and (iii) the *meta*-phenyl protons of ZnP appear separately. We conclude from the aforementioned findings the hindered rotations of the ZnP phenyl groups in the presence of $Ce_2@C_{80}$ and nonequivalent β-pyrrole and phenyl protons. Only a close spatial $Ce_2@I_h$-C_{80}/ZnP proximity, as it is known for several C_{60}/ZnP conjugates,[16] would support such a scenario. In this respect, the 2-oxyethyl butyrate spacer is key to furnish close $Ce_2@I_h$-C_{80}/ZnP contacts. Notably, C_{60}/ZnP conjugates bearing long and flexible spacers give rise to broad and degenerated ^{1}H NMR signals of ZnP protons due to their intramolecular flexibility.[17] In spite of this flexibility, the well-resolved ^{1}H NMR spectra of **1** prompt a rather rigid $Ce_2@I_h$-C_{80}/ZnP conformation. Considering the previous precedents involving C_{60}, it is safe to assume that the giant π-system of C_{80}^{6-} with highly delocalized negative charges further augment such structural arrangements.

A molecular model of **1** (see Figure 3c) reveals (i) a folded conformation, (ii) close C_{80}^{6-}/ZnP proximity, and (iii) asymmetric position of ZnP relative to the Ce−Ce axis.[18] Such an arrangement leads, indeed, to a magnetically and unequivalently affected ZnP.

Electronic $Ce_2@I_h$-C_{80}/ZnP interactions were also inferred from the electronic absorption spectra. Although the Soret band absorption in **1** (i.e., 426 nm) is quite close to that seen in the corresponding C_{60}-ZnP electron donor−acceptor system **3** (i.e., 428 nm),[10] remarkable changes evolve in range of the Q-band absorptions of **1** (i.e., 555 and 594 nm) and **3** (i.e., 551 and 588 nm). Such shifts are particularly helpful because they emerge as sensitive markers for determining the C_{80}^{6-}/ZnP electronic coupling of 400 ± 30 cm^{-1}.[19]

Less pronounced are the differences in the electrochemical assays. Overall, the redox potentials of $Ce_2@I_h$-C_{80} **1** and **2** are quite similar (see Table 2). According to DFT calculations, the LUMO (splitting at −4.50 and −4.01 eV) and HOMO (−5.38 eV) in $Ce_2@I_h$-C_{80} involve $[Ce_2]^{6+}$ and C_{80}^{6-}, respectively.[8b] This places the first/second reduction potential at −0.36/−1.67 V ($Ce_2@I_h$-C_{80}) and −0.42/−1.75 V (**2**) on $[Ce_2]^{6+}$. Oxidation

(13) (a) Wakahara, T.; Kobayashi, J.; Yamada, M.; Maeda, Y.; Tsuchiya, T.; Okamura, M.; Akasaka, T.; Waelchi, M.; Kobayashi, K.; Nagase, S.; Kato, T.; Kako, M.; Yamamoto, K.; Kadish, K. M. *J. Am. Chem. Soc.* **2004**, *126*, 4883–4887. (b) Yamada, M.; Nakahodo, T.; Wakahara, T.; Tsuchiya, T.; Maeda, Y.; Akasaka, T.; Kako, M.; Yoza, K.; Horn, E.; Mizorogi, N.; Kobayashi, K.; Nagase, S. *J. Am. Chem. Soc.* **2005**, *127*, 14570–14571. (c) Yamada, M.; Wakahara, T.; Lian, Y.; Tsuchiya, T.; Akasaka, T.; Waelchli, M.; Mizorogi, N.; Nagase, S.; Kadish, K. M. *J. Am. Chem. Soc.* **2006**, *128*, 1400–1401. (d) Yamada, M.; Wakahara, T.; Tsuchiya, T.; Maeda, Y.; Kako, M.; Akasaka, T.; Yoza, K.; Horn, E.; Mizorogi, N.; Nagase, S. *Chem. Commun.* **2008**, 558–560.

(14) (a) The chemical shift (δ) of a paramagnetic molecule in solution is generally expressed as a sum of three contributions, namely, the diamagnetic (δ_{dia}), Fermi contact (δ_{fc}), and pseudocontact (δ_{pc}) shifts. Note that δ_{fc} makes much less contribution than δ_{pc} in the case of metallofullerene derivatives. The chemical shift (δ) is briefly expressed as eq 1, where r is the distance between Ce and the NMR-active nucleus, θ the angle between the r vector and the vertical axis on which the two Ce atoms are located, and C is a common constant. (b) Bleaney, B. *J. Magn. Reson.* **1972**, *8*, 91–100. (c) Yamada, M.; Okamura, M.; Sato, S.; Someya, C.; Mizorogi, N.; Tsuchiya, T.; Akasaka, T.; Kato, T.; Nagase, S. *Chem.—Eur. J.* **2009**, *15*, 10533–10542.

(15) (a) Haddon, R. C. *Nature* **1995**, *378*, 249–255. (b) Saunder, S M.; Cross, R. J.; Jiménez-Vázquez, H. A.; Shimshi, R.; Khong, A. *Science* **1996**, *271*, 1693–1697.

(16) (a) Imahori, H.; Hagiwara, K.; Aoki, M.; Akiyama, T.; Taniguchi, S.; Okada, T.; Shirakawa, M.; Sakata, Y. *J. Am. Chem. Soc.* **1996**, *118*, 11771–11782. (b) Boyd, P. D. W.; Hodgson, M. C.; Rickard, C. E. F.; Oliver, A. G.; Chaker, L.; Brothers, P. J.; Bolskar, R. D.; Tham, F. S.; Reed, C. A. *J. Am. Chem. Soc.* **1999**, *121*, 10487–10495. (c) Schuster, D. I. *Carbon* **2000**, *38*, 1607–1614. (d) Schuster, D. I.; Jarowski, P. D.; Kirschner, A. N.; Wilson, S. R. *J. Mater. Chem.* **2002**, *12*, 2041–2047. (e) Pérez, E. M.; Martín, N. *Chem. Soc. Rev.* **2008**, *37*, 1512–1519. (f) Lembo, A.; Tagliatesta, P.; Cicero, D.; Leoni, A.; Salvatori, A. *Org. Biomol. Chem.* **2009**, *7*, 1093–1096.

(17) (a) Dietel, E.; Hirsch, A.; Zhou, J.; Rieker, A. *J. Chem. Soc., Perkin Trans. 2* **1998**, 1357–1364. (b) MacMahon, S.; Wilson, S. R.; Schuster, D. I. *Proc. Elec. Chem. Soc.* **2000**, *8*, 155–160. (c) MacMahon, S.; Fong, R.; Baran, P. S.; Safonov, I.; Wilson, S. R.; Schuster, D. I. *J. Org. Chem.* **2001**, *66*, 5449–5455.

(18) Molecular model of **1** shows an energy minimized structure obtained with simulated annealing plus geometry optimization using the Forcite of MS modeling. The $Ce_2@I_h$-C_{80} atomic positions are imported from the X-ray structure of **2** and kept fixed during the modeling.

(19) Guldi, D. M.; Hirsch, A.; Scheloske, M.; Dietel, E.; Troisi, A.; Zerbetto, F.; Prato, M. *Chem.—Eur. J.* **2003**, *9*, 4968–4979.

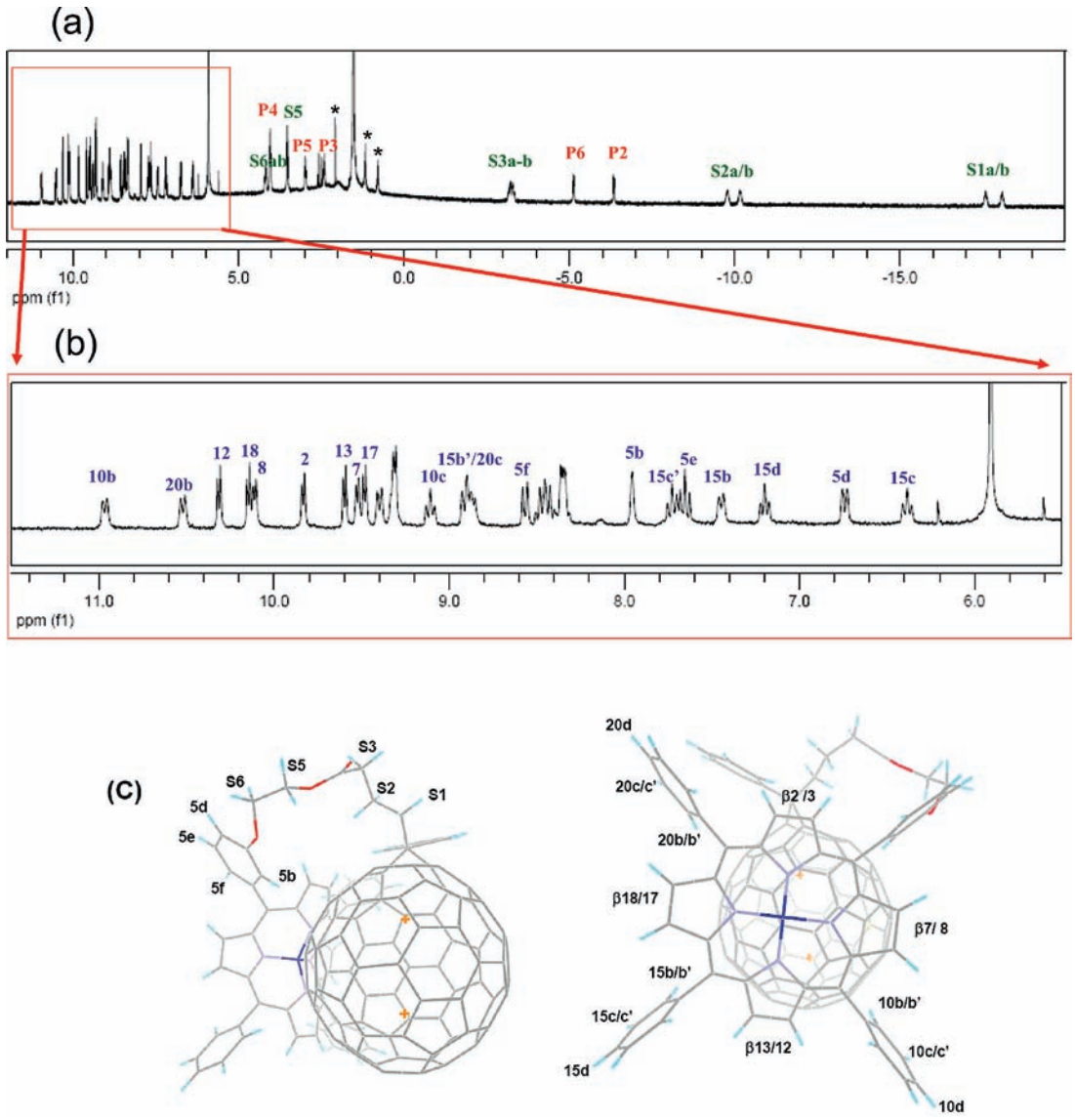

Figure 3. (a,b) ^{1}H NMR spectra (300 MHz) of **1** in $C_2D_2Cl_4$ at 293 K with the marked signals (*) originating from impurities. (c) Two side views of a molecular model of **1**.[18] The assignments are based on the 2D-DQFCOSY and NOESY experiments.

Table 2. Redox Potentials of **1** and Reference Compounds[a]

	E_4^{ox}	E_3^{ox}	E_2^{ox}	E_1^{ox}	E_1^{red}	E_2^{red}	E_3^{red}	E_4^{red}
$Ce_2@C_{80}$			0.95	0.55	−0.36	−1.67	−2.21	
2			0.91	0.48	−0.42	−1.75	−2.23	
1	0.98/0.85[b]	0.63	0.55	0.35	−0.43	−1.76	−1.91	−2.25[c]
ZnP		0.65		0.39			−1.94	−2.27

[a] All of the potentials, in volts, were measured relative to the $Fc^{0/+}$. [b] Splitted one-electron oxidation process. [c] Two-electron reduction process.

at around +0.5 V occurs, on the other hand, exclusively at C_{80}^{6-}. Subtle differences were also evidenced for the reduction of ZnP in **1** (−1.91/−2.25 V) and its reference (−1.94/−2.27 V) as well as the oxidation of ZnP in **1** (0.35/0.63 V) and its reference (0.39/0.65 V).

Insights into excited state interactions between $Ce_2@I_h$-C_{80} and ZnP came from steady-state fluorescence measurements. In this context, pristine ZnP evolved as a particular convenient marker owing to its high and nearly solvent-independent fluorescence quantum yield of 0.04.[20] At first glance, the ZnP-centered fluorescence with maxima at 605 and 650 nm in **1** is nearly solvent-independently quenched. Quantum yields of ~0.004 suggest a "through-space" mechanism that is operative in deactivating the ZnP singlet excited state, either charge or energy transfer. The view of through-space interactions is in sound agreement with the conclusion of the spectroscopic characterization (vide supra). A closer analysis (see Figure 4) brings nevertheless some subtle changes to light. In toluene (0.002) and THF (0.004), the quenching appears to be stronger than in benzonitrile (0.006) and DMF (0.006). We assign this preliminary data to a change in electronic coupling between electron donor and electron acceptor.

To further exploit interactions between photoexcited $Ce_2@I_h$-C_{80} and ZnP, we turned to complementary transient absorption measurements. Up front, the excited state properties of pristine ZnP (Figure 5) and **2** (Figure 6) shall be discussed because they serve as important reference points for the interpretation of **1**. The differential absorption changes recorded upon excitation of the ZnP reference are characterized by bleaching of the ZnP Q-band absorption at 550 nm and broad absorption between

(20) D'Souza, F.; Ito, O. *Chem. Commun.* **2009**, 4913–4928.

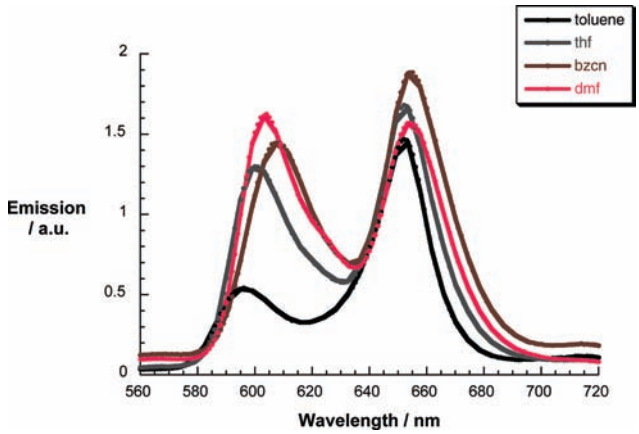

Figure 4. Steady-state fluorescence spectra of **1** in solvents of different polarity with matching absorption at the excitation wavelength (i.e., $OD_{426nm} = 0.1$).

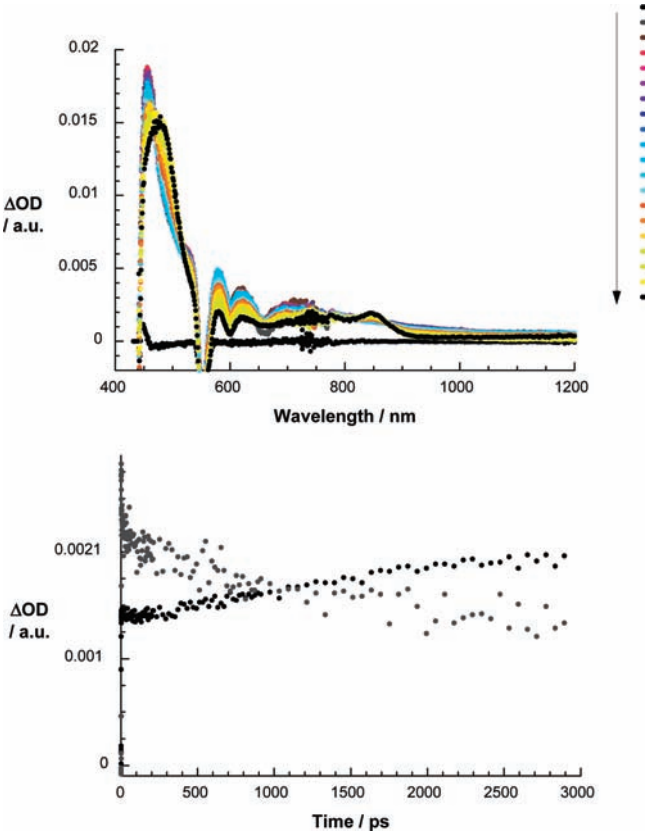

Figure 5. Top: Differential absorption spectra (visible and near-infrared) obtained upon femtosecond flash photolysis (387 nm) of pristine ZnP ($\sim 10^{-5}$ M) in argon-saturated toluene with several time delays between 0 and 3000 ps at room temperature (see legend for details about time progression). Bottom: Time-absorption profiles of the spectra shown above at 700 and 850 nm monitoring the intersystem crossing.

570 and 750 nm.[20] These spectral attributes reflect the ZnP singlet excited state and decay slowly (4.0×10^8 s^{-1}) to the energetically lower-lying triplet excited state with a characteristic maximum at 840 nm predominantly via intersystem crossing. On the contrary, the singlet excited state features of **2** are dominated by a rather broad singlet−singlet transition that spans from 400 to 800 nm. The latter undergoes a rapid intersystem crossing (3×10^{10} s^{-1}) to yield the triplet manifold. Spectroscopically, a 550 nm maximum is noted for the triplet.

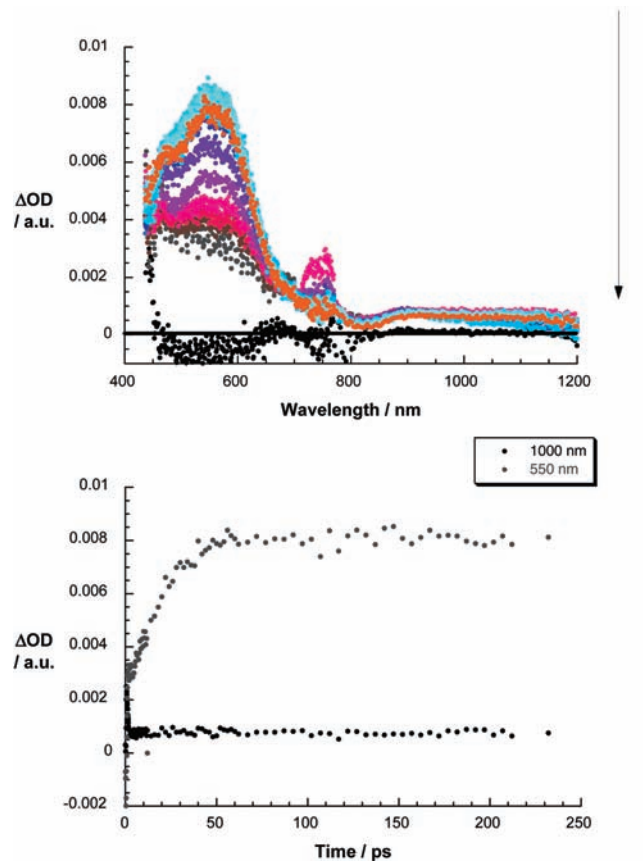

Figure 6. Top: Differential absorption spectra (visible and near-infrared) obtained upon femtosecond flash photolysis (387 nm) of **2** ($\sim 10^{-5}$ M) in argon-saturated toluene with several time delays between 0 and 250 ps at room temperature (see legend for details about time progression). Bottom: Time-absorption profiles of the spectra shown above at 550 and 1000 nm monitoring the intersystem crossing.

In the femtosecond transient absorption measurements of **1**, immediately after the laser excitation, the strong singlet−singlet absorptions of ZnP are discernible. This confirms, despite the presence of $Ce_2@I_h$-C_{80}, the successful formation of the ZnP singlet excited states. Instead of seeing, however, the slow growth of the ZnP triplet features, the singlet−singlet absorptions decay with accelerated dynamics in toluene (1.2×10^{12}), THF (1.3×10^{12}), benzonitrile (1.4×10^{12}), and DMF (2.3×10^{12} s^{-1}). Spectroscopically, the transient absorption changes taken after the completion of the decay bear no resemblance to the ZnP triplet excited state. Instead, in THF, the new transient, as shown in Figure 7, is ascribed to that of the $(Ce_2@I_h\text{-}C_{80})^{\bullet-}$-$(ZnP)^{\bullet+}$ radical ion pair state. In the visible region, the broad absorption in the 600−700 nm region corresponds to the one-electron oxidized ZnP. On the other hand, in the near-infrared region, the broad maximum between 900 and 1200 nm resembles the spectroelectrochemical signature of the one-electron reduced $Ce_2@I_h$-C_{80} (see Figure S1 in the Supporting Information).

Interestingly, a closer inspection of the transient absorption changes seen in benzonitrile and DMF reveal characteristics that differ from those seen in toluene and THF. In particular, Figure 8 displays that in the visible region new minima and maxima develop at 555/595 nm and 465/530/580 nm, respectively. Notable is the sharp discrepancy relative to the features known for the one-electron oxidized ZnP.

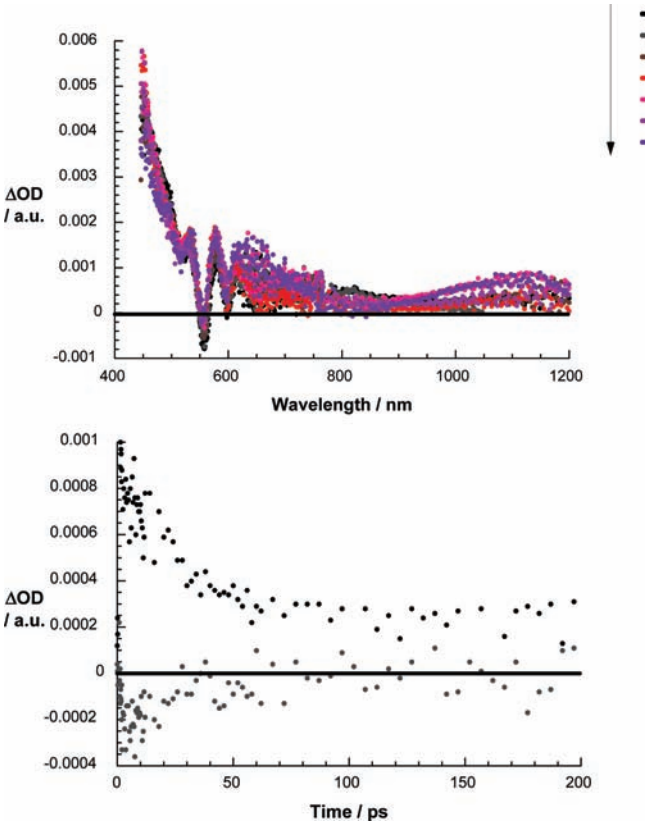

Figure 7. Top: Differential absorption spectra (visible and near-infrared) obtained upon femtosecond flash photolysis (387 nm) of **1** ($\sim 10^{-5}$ M) in argon-saturated THF several time delays between 0 and 50 ps at room temperature (see legend for details about time progression). Bottom: Time-absorption profiles of the spectra shown above at 555 and 580 nm, monitoring the charge separation.

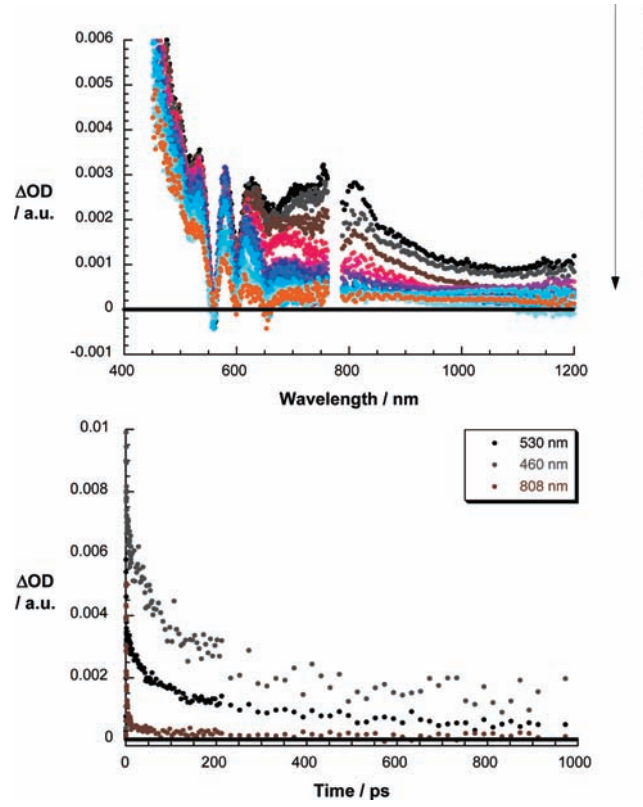

Figure 8. Top: Differential absorption spectra (visible and near-infrared) obtained upon femtosecond flash photolysis (387 nm) of **1** ($\sim 10^{-5}$ M) in argon-saturated DMF with several time delays between 0 and 1000 ps at room temperature (see legend for details about time progression). Bottom: Time-absorption profiles of the spectra shown above at 460, 530, and 808 nm, monitoring the charge separation and charge recombination.

Extending our spectroelectrochemical investigations into the cathodic region shed light onto the nature of this transient (see Figure 9). When applying a potential of −1.5 V (sufficient to reduce ZnP), the corresponding spectral changes are an exact match of what was observed during the femtosecond transient absorption measurements. Likewise, in the near-infrared, an apparent mismatch with the one-electron reduced $Ce_2@I_h$-C_{80} is seen. Only anodic conditions in the spectroelectrochemistry led to the expected agreement, that is, a maximum at 860 nm (see Figure 9). In other words, the close spectral resemblance of spectroelectrochemistry and photochemistry prompts the unprecedented formation of the $(Ce_2@I_h\text{-}C_{80})^{\bullet+}$-$(ZnP)^{\bullet-}$ radical ion pair state. The time absorption profiles indicate that this highly exergonic state is metastable. In fact, multiwavelength analyses provide lifetimes of 55 and 115 ps in benzonitrile and DMF, respectively. It is, however, the triplet excited state of $Ce_2@I_h$-C_{80} that is formed as the stable product of charge recombination. Support for this assumption came from complementary nanosecond experiments, where a long-lived transient is seen, in agreement with the reference experiments performed with **2**.

A likely rationale for the change in reactivity, that is, toluene/THF versus benzonitrile/DMF, is associated with the energies of the $(Ce_2@I_h\text{-}C_{80})^{\bullet-}$-$(ZnP)^{\bullet+}$ (0.78 eV) and $(Ce_2@I_h\text{-}C_{80})^{\bullet+}$-$(ZnP)^{\bullet-}$ (2.3 eV) radical ion pair states. Reduction of the $[Ce_2]^{6+}$ cluster, which is, on one hand, highly localized and collinearly arranged relative to the quaternary bridge carbon but, on the other hand, weakly coupled electronically to the electron-donating ZnP, requires a sufficient free energy change (i.e., $-\Delta G^\circ$). This is unmistakably secured in toluene (−1.18 eV), THF (−1.47 eV), benzonitrile (−1.56 eV), and DMF (−1.57 eV). In contrast, the ZnP singlet excited state (2.1 eV) renders in *ortho*-dichlorobenzene as energetically insufficient for driving the oxidation of C_{80}^{6-} and the simultaneous reduction of ZnP (2.3 eV).

The energy diagram in Figure 10 summarizes the aforementioned. In particular, to bring the $(Ce_2@I_h\text{-}C_{80})^{\bullet+}$-$(ZnP)^{\bullet-}$ radical ion pair state energy in **1**, however, below that of the singlet excited state of ZnP and, in turn, to activate this charge transfer pathway necessitates solvent stabilization (i.e., $\Delta G_{solvent}$), benzonitrile (0.28 eV) and DMF (0.31 eV). The strongly exothermic $(Ce_2@I_h\text{-}C_{80})^{\bullet-}$-$(ZnP)^{\bullet+}$ radical ion pair state formation is compensated within the framework of a nonadiabatic charge transfer by an C_{80}^{6-}/ZnP electronic matrix element as the sum of good overlap and short distance that exceeds that for $[Ce_2]^{6+}$/ZnP. Please note that the $Ce_2@I_h$-C_{80} singlet excited state energy (1.0 eV) fails to play any significant function in any charge transfer chemistry.

Conclusions

To summarize, our investigations have shed light on the nature of $Ce_2@I_h$-C_{80} in charge transfer chemistry. In particular, a remarkable electron donor−acceptor conjugate, involving $Ce_2@I_h$-C_{80} and ZnP, has been synthesized and characterized. Detailed spectroscopic analyses revealed unusually strong $Ce_2@I_h$-C_{80}/ZnP interactions, despite employing a flexible 2-oxyethyl butyrate linkage. These interactions are driven and enforced by a giant π-system with highly delocalized negative

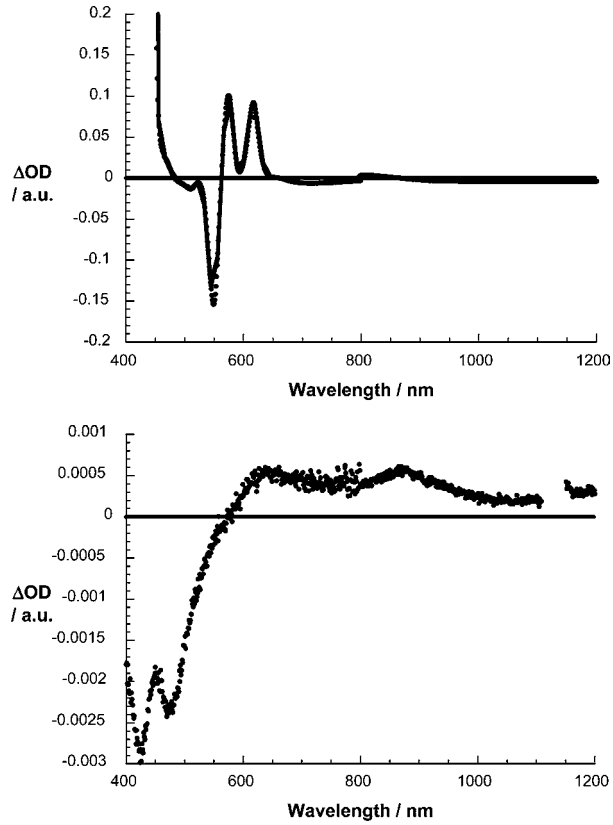

Figure 9. Top: Differential absorption spectrum (visible and near-infrared) obtained upon electrochemical reduction of ZnP ($\sim 10^{-5}$ M) at an applied bias of −1.6 V in argon-saturated *o*-dichlorobenzene at room temperature. Bottom: Differential absorption spectrum (visible and near-infrared) obtained upon electrochemical oxidation of **2** ($\sim 10^{-5}$ M) at an applied bias of +0.6 V in argon-saturated *o*-dichlorobenzene at room temperature.

charges. Most impressive is the unprecedented change in charge transfer chemistry in toluene/THF versus benzonitrile/DMF. In this context, the different strength in electronic coupling, $[Ce_2]^{6+}$/ZnP versus C_{80}^{6-}/ZnP, affects the charge transfer kinetics and the charge transfer mechanism, that is, formation of $(Ce_2@I_h\text{-}C_{80})^{\bullet-}$-$(ZnP)^{\bullet+}$ or $(Ce_2@I_h\text{-}C_{80})^{\bullet+}$-$(ZnP)^{\bullet-}$. Especially the latter reactivity pattern renders $Ce_2@I_h\text{-}C_{80}$ a promising and unprecedented p-type fullerene material for a solar energy conversion system. Likewise, it creates new possibilities for fundamental process of water oxidation triggered by light.[21]

Experimental Section

Spectroscopy: All NMR spectra were recorded on a Bruker AC 300 spectrometer or Bruker AV 500 spectrometer with a CryoProbe system, locked on deuterated solvents and referenced to the solvent peak. The 1D and 2D experiments (COSY, DQF-COSY, NOESY, HMQC, and HSQC) were performed by means of standard experimental procedures of the Bruker library. Absorption spectra of all samples were recorded in toluene with a Shimadzu UV-3150 spectrometer using a quartz cell and 1 nm resolution. Matrix-assisted laser desorption−ionization time-of-flight (MALDI-TOF) mass spectra were recorded with a Bruker BIFLEX-III mass spectrometer using 1,1,4,4-tetraphenyl-1,3-butadiene as the matrix. The measurements were performed in both positive and negative ion modes.

Steady-State Emission: The spectra were recorded on a FluoroMax 3 fluorometer (vis detection) and on a Fluorolog spectrometer (NIR detection). Both spectrometers were built by HORIBA JobinYvon. The measurements were carried out at room temperature.

Time-Resolved Absorption: Femtosecond transient absorption studies were performed with 387 nm laser pulses (1 kHz, 150 fs pulse width) from an amplified Ti:sapphire laser system (Clark-MXR, Inc.), and the laser energy was 200 nJ.

Electrochemistry: Differential pulse voltammetry (DPV) and cyclic voltammetry (CV) were carried out in *o*-DCB using a BAS CW-50 instrument. A conventional three-electrode cell consisting of a platinum working electrode, a platinum counter-electrode, and a saturated calomel reference electrode (SCE) was used for both measurements. $(n\text{-}Bu)_4NPF_6$ was used as the supporting electrolyte. All potentials were recorded against a SCE reference electrode and corrected against Fc/Fc^+. DPV and CV were measured at a scan rate of 20 and 50 mV s^{-1}, respectively. The spectroelectrochemical measurements were done on a Varian Cary 5000 UV−vis−NIR spectrophotometer connected to a Princeton PGstat 263A using a home-made cell with three-electrode configuration. A light transparent platinum gauze, a platinum plate, and a silver wire were employed as the working, counter, and reference electrodes, respectively, in an analyte solution of *o*-dichlorobenzene containing 0.2 M tetrabutylammonium perchlorate supporting electrolyte. The absorbances of the analyzed compounds were fixed between 0.1 and 0.15. The path length of the cell was determined to be 2.3 mm. The desired potential was applied, and the system output was measured for around 20 cycles. The difference between the spectrum with and without an applied potential was plotted as ΔOD.

Radiolysis: Pulse radiolysis experiments were performed using 50 ns pulses of 15 MeV electrons from a linear electron accelerator (LINAC). Dosimetry was based on the oxidation of SCN^- to $(SCN)_2^{\bullet-}$ which in aqueous, N_2O-saturated solution takes place with $G \approx 6$ (G denotes the number of species per 100 eV, or the approximate μM concentration per 10 J absorbed energy). The radical concentration generated per pulse was varied between 1×10^{-6} and 3×10^{-6} M.

Materials: All chemicals were of reagent grade and purchased from Wako. $Ce_2@I_h\text{-}C_{80}$ was produced and separated according to a previously reported method.[5] Preparative and analysis HPLC was performed on Buckyprep column (ø25 × 100 mm, Cosmosil) and Buckyprep column, 5PYE column, and Buckyclutcher column (ø4.6 × 100 mm, Cosmosil), respectively. Toluene was used as eluent.

Synthesis: The synthesis of the diazo precursor (6•2H) and dyad **3** are described in the Supporting Information.[10]

1-(3-(Methoxycarbonyl)propyl)-1-phenyl[6,6]$Ce_2@C_{81}$ (2). Methyl 4-benzoylbutyrate *p*-tosylhydrazone (1.4 mg, 0.0037 mmol) and a small amount of NaOMe (ca. 0.5 mg, 0.0092 mmol) were dissolved in 60 μL of dry pyridine under N_2 for 10 min. A solution of 1.5 mg (0.0012 mmol) of $Ce_2@C_{80}$ in 2.5 mL of *o*-DCB was added, and the mixture was stirred at 75 °C for 2 h. After cooling to room temperature, pyridine was removed under vacuum. The reaction mixture was filtered, and *o*-DCB was removed under vacuum. A solution of CS_2/acetone (v/v = 1/1) with 3−4 μL of $CHCl_2COOH$ was added to dissolve the solid. The mixture was stirred for 15 min, and 10 mL of toluene was added. After removing CS_2/acetone by vacuum, the resulting toluene solution was subjected to HPLC analysis and separation. **2** was separated as a predominant product: yield ca. 62% based on consumed $Ce_2@C_{80}$; ^{1}H NMR (300 MHz, $C_2D_2Cl_4$, 293 K) (paramagnetic) δ = 4.10 (t, ^3J = 7.04 Hz, 1H, *p*-Ar*H*), 3.13 (t, ^3J = 7.71 Hz, 1H, *m*-Ar*H*), 2.57 (t, ^3J = 7.61 Hz, 1H, *m*-Ar*H*), 2.23 (s, 3H, OCH_3), −3.43 (t, ^3J = 7.61 Hz, 2H, CH_2CH_2CO), −4.87 (d, ^2J = 8.11 Hz, 1H, *o*-Ar*H*), −6.09 (d, ^2J = 8.42 Hz, 1H, *o*-Ar*H*), −9.74 (br m, $1H_a$, $PhCCH_2CH_2$), −10.09 (br m, H_b, $PhCCH_2CH_2$), −17.43 (br t, H_a, $PhCCH_2CH_2$), −17.96 (br t, H_b, $PhCCH_2CH_2$); ^{13}C NMR (125 MHz, $C_2D_2Cl_4$, 288 K) (paramagnetic) δ = 198.50, 198.29, 194.12, 192.80, 189.66, 186.84, 186.73, 183.84, 183.42, 174.74, 174.48, 173.15, 172.73, 172.20, 171.71, 171.65, 171.17, 170.46, 169.43 (2C), 169.32, 169.16 (C═O), 165.90, 164.77, 161.99, 161.80, 160.77, 160.35, 159.92, 159.74, 159.53, 159.48, 158.25, 157.81, 157.15, 156.80 (2C), 156.12, 154.84, 154.69, 150.48, 150.35, 149.14, 148.89, 148.60, 148.36, 147.35, 147.24, 146.43, 146.24, 146.11, 144.57, 144.53,

(21) Messinger, J. *ChemSusChem.* **2009**, *2*, 47–48.

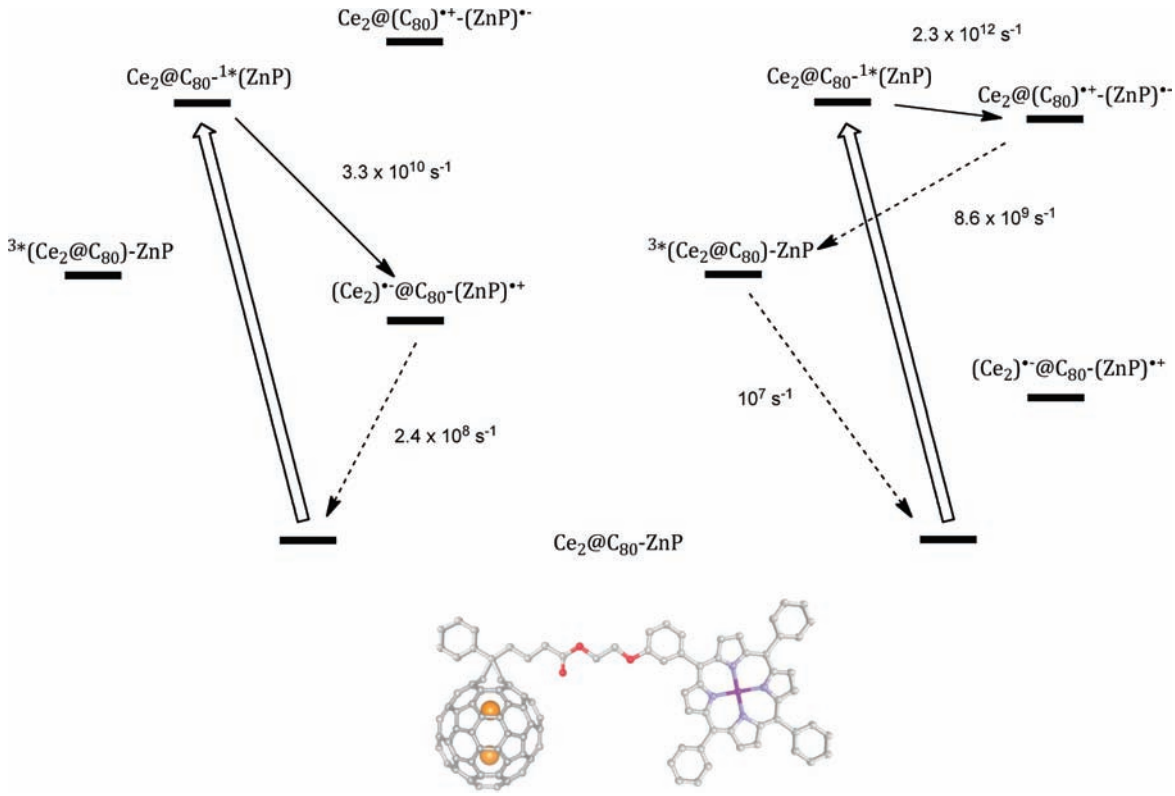

Figure 10. Energy diagram for **1** illustrating the different excited state deactivation pathways that lead in toluene and THF (left-hand side) and benzonitrile and DMF (right-hand side) to different charge transfer products.

142.98, 141.99, 138.28, 137.95, 137.59, 137.44, 135.86, 133.75, 133.51, 129.28, 129.07, 127.49 (Ph), 125.04, 124.62, 123.28 (Ph), 122.80 (Ph), 122.38 (Ph), 118.94, 118.81, 114.70 (Ph), 114.02 (Ph), 103.24, 99.95, 93.27, 87.34, 82.89, 82.20, 81.99, 77.76, 50.61 (OCH_3), 35.70, 26.78 (CH_2CO_2), 23.55 (br, $CH_2CH_2CO_2$), 9.21, 7.85, 4.81 (br, $PhCCH_2$), −3.58 (spiro carbon); MS (MALDI-TOF) m/z = 1429.52 $[M]^+$, calcd for $Ce_2C_{92}H_{14}O_2$ m/z = 1429.91.

$Ce_2@I_h$-C_{80}-ZnP (1). 6•2H (4.5 mg, 4.1×10^{-3} mmol) and a small amount of NaOMe (ca. 0.5 mg, 0.0092 mmol) were dissolved in pyridine (150 μL) and stirred for 15 min under N_2. Then, $Ce_2@C_{80}$ (1.13 mg, 9.1×10^{-4} mmol) in 1.5 mL of *o*-DCB was added. The mixture was stirred at 80 °C for 2 h under N_2. After cooling the reaction mixture, 500 μL of saturated $Zn(OAc)_2$/MeOH was added and the mixture was stirred for 30 min. After removing the solvent under vacuum, the solid was dissolved in toluene and filtered. The final reaction mixture underwent HPLC analysis. **1** was facilely separated and purified by two-step HPLC process: yield ca. 40−50% based on consumed $Ce_2@C_{80}$; ^{1}H NMR (300 MHz, $C_2D_2Cl_4$, 293 K) (paramagnetic) δ = 10.98 (d, ^2J = 7.30 Hz, 1H), 10.53 (d, ^2J = 7.63 Hz, 1H), 10.32 (d, ^2J = 4.76 Hz, 1H-β), 10.16 (d, ^2J = 4.77 Hz, 1H-β), 10.12 (d, ^2J = 4.75 Hz, 1H-β), 9.84 (d, ^2J = 4.74 Hz, 1H-β), 9.61 (d, ^2J = 4.76 Hz, 1H-β), 9.53 (d, ^2J = 4.74 Hz, 1H-β), 9.49 (d, ^2J = 4.77 Hz, 1H-β), 9.41 (d, ^2J = 6.98 Hz, 1H), 9.32 (m, 2H), 9.11 (t, ^3J = 7.01 Hz, 1H), 8.90 (m, 2H), 8.58 (d, ^2J = 5.91 Hz, 1H), 8.48 (t, ^3J = 7.95 Hz, 1H), 8.42 (t, ^3J = 7.94 Hz, 1H), 8.35 (m, 2H), 7.95 (s, 1H), 7.73 (t, ^3J = 7.79 Hz, 1H), 7.65 (t, ^3J = 8.11 Hz, 1H), 7.46 (d, ^2J = 7.46 Hz, 1H), 7.20 (t, ^3J = 7.01 Hz, 1H), 6.75 (d, ^2J = 8.25 Hz, 1H), 6.38 (t, ^3J = 7.46 Hz, 1H), 4.17 (br, 1H), 4.04 (m, 2H), 3.53 (br, 2H), 2.98 (t, ^3J = 7.70 Hz, 1H, *m*-Ar*H*), 2.41 (t, ^3J = 7.00 Hz, 1H, *m*-Ar*H*), −3.20 (m, $1H_a$, $CH_2CH_2CO_2$), −3.28 (m, $1H_b$, $CH_2CH_2CO_2$), −5.12 (d, ^2J = 8.45 Hz, 1H, *o*-Ar*H*), −6.34 (d, ^2J = 7.83 Hz, 1H, *o*-Ar*H*), −9.79 (br m, $1H_a$, CH_2CH_2CO), −10.17 (br m, $1H_b$, CH_2CH_2CO), −17.60 (br t, $1H_a$, $PhCCH_2CH_2$), −18.10 (br t, $1H_b$, $PhCCH_2CH_2$); ^{13}C NMR (125 MHz, $C_2D_2Cl_4$, 288 K) (paramagnetic) δ = 196.20, 194.79, 192.79, 191.60, 190.89, 187.21 (2C), 183.59, 183.10, 181.96, 179.93, 173.50, 172.41, 171.07, 170.96, 170.70, 169.57, 169.01, 168.91, 168.76, 168.49 (C═O), 168.37, 167.29, 166.97, 164.59, 162.81, 161.38, 159.47, 159.40, 158.46, 158.38, 158.09, 157.16, 156.79, 156.72, 156.57, 156.41, 155.54, 155.36, 155.19, 154.71, 153.92, 153.21, 153.05, 153.00, 152.92, 152.60, 152.51, 152.48, 152.22, 152.09, 148.92, 148.37, 148.18, 147.52, 147.14, 146.29, 145.87, 145.44, 145.21, 145.00, 144.62, 144.32, 143.92, 143.61, 143.01, 142.01, 141.92, 141.14, 137.02, 136.89, 136.46, 136.29, 136.17, 135.96, 135.38, 134.85, 134.60, 134.11, 133.96, 133.91, 133.73, 133.63, 133.58, 133.37, 133.09, 132.88, 132.39, 129.32, 129.24, 128.70, 128.60, 128.55, 128.40, 127.84, 127.71, 127.58, 127.29 (Ph), 126.94, 126.81, 126.25, 124.62, 124.28, 123.81, 123.69, 123.27, 123.18, 123.10, 122.81 (Ph), 122.69 (Ph), 122.38, 119.09, 117.31, 114.72 (Ph), 114.08 (Ph), 112.64, 104.65, 101.76, 99.32, 92.94, 87.04, 83.86, 83.26, 81.61, 65.91 (OCH_2), 62.05 (CH_2OCO), 37.79, 27.29 (CH_2CO_2), 23.05 (br, $CH_2CH_2CO_2$), 10.05, 8.57, 4.83 (br, $PhCCH_2$), −0.96 (spiro carbon); MS (MALDI-TOF) m/z = 2136.18 $[M + 2H]^+$, calcd for $Ce_2C_{137}H_{42}N_4O_3Zn$ m/z = 2134.06.

Crystallography: Single crystals of **2**•2CS_2 suitable for X-ray diffraction were obtained from slow diffusion between **2**/CS_2 and hexane. Data were collected on a Rigaku Raxis-Rapid IP diffractometer using monochromatized Mo Kα radiation (λ = 0.71075 Å) at 120 K. The structure was solved by direct method and refined by the full-matrix least-squares method. All non-hydrogen atoms were refined with anisotropic thermal parameters, whereas all hydrogen atoms were calculated using a riding model and were included in the structure factor calculation.

Acknowledgment. This work was supported in part by the Deutsche Forschungsgemeinschaft, Cluster of Excellence "Engineering of Advanced Materials", FCI, the Office of Basic Energy Sciences of the U.S., a Grant-in-Aid for Scientific Research on Innovative Areas (No. 20108001, "pi-Space"), a Grant-in-Aid for Scientific Research (A) (No. 20245006), the 21st Century COE

Program, The Next Generation Super Computing Project (Nanoscience Project), Nanotechnology Support Project, and a Grant-in Aid for Scientific Research on Priority Area (Nos. 20036008, 20038007) from the Ministry of Education, Culture, Sports, Science, and Technology of Japan. H.N. and M.Y. thank the Japan Society for the Promotion of Science (JSPS) for the Research Fellowship for Young Scientists. L.F. also thanks the National Natural Science Foundation of China (20702053). We also thank the MICINN of Spain (projects CTQ2008-00795/BQU and Consolider-Ingenio 2010C-07-25200), and the CAM (project P-PPQ-000225-0505).

Supporting Information Available: Differential absorption spectra of one-electron reduced $Ce_2@I_h$-C_{80}. Synthesis of diazo precursor 6•2H and **3**. HPLC profiles and MALDI-TOF spectra of **2** and **1**. Various NMR spectra of **2** and **1**. Differential pulse voltammetry (DPV) and cyclic voltammograms (CV) of **2** and **1**. This material is available free of charge via the Internet at http://pubs.acs.org.

JA101856J